

2018

# Structural features and domain movements controlling substrate binding and cofactor specificity in class II HMG-CoA reductase

Bradley R. Miller

*Bryn Mawr College*, [bmiller@brynmawr.edu](mailto:bmiller@brynmawr.edu)

Yan Kung

*Bryn Mawr College*, [ykung@brynmawr.edu](mailto:ykung@brynmawr.edu)

[Let us know how access to this document benefits you.](#)

Follow this and additional works at: [https://repository.brynmawr.edu/chem\\_pubs](https://repository.brynmawr.edu/chem_pubs)

 Part of the [Biochemistry Commons](#), [Other Biochemistry, Biophysics, and Structural Biology Commons](#), and the [Structural Biology Commons](#)

---

## Citation

Miller, Bradley R. and Kung, Yan, "Structural features and domain movements controlling substrate binding and cofactor specificity in class II HMG-CoA reductase" (2018). *Chemistry Faculty Research and Scholarship*. 27.  
[https://repository.brynmawr.edu/chem\\_pubs/27](https://repository.brynmawr.edu/chem_pubs/27)

This paper is posted at Scholarship, Research, and Creative Work at Bryn Mawr College. [https://repository.brynmawr.edu/chem\\_pubs/27](https://repository.brynmawr.edu/chem_pubs/27)

For more information, please contact [repository@brynmawr.edu](mailto:repository@brynmawr.edu).

# Structural Features and Domain Movements Controlling Substrate Binding and Cofactor Specificity in Class II HMG-CoA Reductase

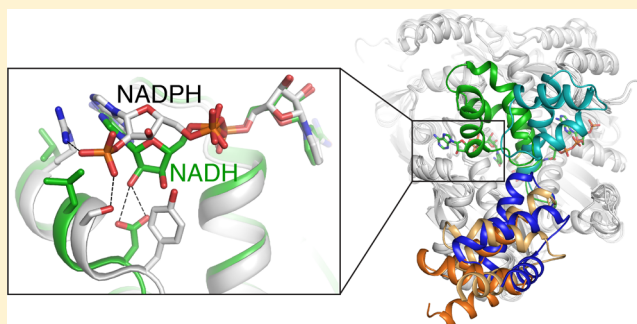
Bradley R. Miller and Yan Kung\*<sup>1b</sup>

Department of Chemistry, Bryn Mawr College, 101 North Merion Avenue, Bryn Mawr, Pennsylvania 19010, United States

## Supporting Information

**ABSTRACT:** The key mevalonate pathway enzyme 3-hydroxy-3-methylglutaryl coenzyme A (HMG-CoA) reductase (HMGR) uses the cofactor NAD(P)H to reduce HMG-CoA to mevalonate in the production of countless metabolites and natural products. Although inhibition of HMGR by statin drugs is well-understood, several mechanistic details of HMGR catalysis remain unresolved, and the structural basis for the wide range of cofactor specificity for either NADH or NADPH among HMGRs from different organisms is also unknown. Here, we present crystal structures of HMGR from *Streptococcus pneumoniae* (SpHMGR) alongside kinetic data of the enzyme's cofactor preferences. Our structure of SpHMGR

bound with its kinetically preferred NADPH cofactor suggests how NADPH-specific binding and recognition are achieved. In addition, our structure of HMG-CoA-bound SpHMGR reveals large, previously unknown conformational domain movements that may control HMGR substrate binding and enable cofactor exchange without intermediate release during the catalytic cycle. Taken together, this work provides critical new insights into both the HMGR reaction mechanism and the structural basis of cofactor specificity.



HMGR catalyzes the rate-limiting step of the mevalonate pathway, which is found in all kingdoms of life and is responsible for the biosynthesis of an enormously wide range of molecules, from steroids such as cholesterol to isoprenoids, which make up the largest and most diverse class of natural products. Its key role in the biosynthesis of steroids makes HMGR the target of cholesterol-lowering statin drugs. HMGR performs the four-electron reduction of HMG-CoA to mevalonate and CoA using 2 equiv of the redox cofactor NAD(P)H. The enzyme has evolved into two distinct classes,<sup>1–3</sup> where class I HMGRs are present in eukaryotes and in some bacteria and archaea, while class II enzymes are found in only bacteria and archaea. Although both HMGR classes exhibit similar overall folds, with active sites located at a homodimeric interface, there are many significant differences, including those in catalytic regions of the protein.<sup>2</sup>

Class I and class II HMGRs also differ in their NAD(P)H cofactor preferences: although all class I HMGRs, including the human enzyme, utilize NADPH exclusively, class II HMGRs display a wide range of cofactor specificities. Some class II enzymes use only NADH, including the HMGRs from *Pseudomonas mevalonii* (PmHMGR)<sup>4</sup> and *Burkholderia cenocepacia*,<sup>5</sup> while others use only NADPH, such as HMGR from *Enterococcus faecalis*.<sup>6</sup> Other class II HMGRs are able to use both NADH and NADPH, often with weak or strong preferences for one cofactor or the other, including HMGRs from *Staphylococcus aureus*,<sup>7</sup> *Listeria monocytogenes*,<sup>8</sup> and *Archaeoglobus fulgidus*.<sup>9</sup>

Despite the fact that HMGR inhibition by statins is well-understood, the molecular details of the HMGR catalytic mechanism remain somewhat enigmatic.<sup>10</sup> Current proposals suggest that HMG-CoA is first reduced to a mevaldyl-CoA intermediate using the first equivalent of NAD(P)H. The order of the next two steps is uncertain. Oxidized NAD(P)<sup>+</sup> must be exchanged for a second equivalent of NAD(P)H, and mevaldyl-CoA is also cleaved to form a mevaldehyde intermediate and CoA. Lastly, mevaldehyde is reduced to mevalonate by the second NAD(P)H, and the final products are released.

Interestingly, HMGR can also produce mevalonate if provided with its mevaldyl-CoA or mevaldehyde intermediates,<sup>11,12</sup> skipping the first reduction step. However, when HMG-CoA is the substrate, neither intermediate is released during the catalytic cycle;<sup>10,13–15</sup> instead, the enzyme waits until the second reduction step is complete to release the final products. How HMGR is able to trigger and accomplish cofactor exchange during the reaction without releasing the bound intermediates is not known. In addition, the structural basis for class II HMGR's wide range of cofactor specificity is also unclear. Greater knowledge of the structural features that control substrate and cofactor binding in class II HMGR not only would provide insight into its catalytic mechanism but

Received: October 3, 2017

Published: December 11, 2017



also may enable the development of drugs that target this crucial metabolic enzyme in human pathogens.

To date, crystal structures for only two class II HMGRs have been determined, namely, the NADH-specific PmHMGR and HMGR from the major human pathogen *Streptococcus pneumoniae* (SpHMGR). SpHMGR inhibition has been previously studied,<sup>16</sup> but its cofactor preferences have not been determined until now. For PmHMGR, many structures are available,<sup>17–19</sup> including the ternary complex depicting the enzyme bound simultaneously with both the cofactor in its oxidized form, NAD<sup>+</sup>, and the substrate HMG-CoA [Protein Data Bank (PDB) entry 1QAX] or the substrate analogue dithio-HMG-CoA (PDB entry 4I4B). For SpHMGR, two structures have been determined in the absence of any bound ligands (PDB entries 3QAE and 3QAU). Interestingly, a C-terminal domain that is disordered in the vast majority of HMGR structures, indicating a high degree of domain mobility, was ordered in structures of the PmHMGR ternary complex and apo-SpHMGR. Here, the C-terminal domain in apo-SpHMGR was flipped away from the substrate- and cofactor-binding sites, giving rise to an “open” conformation, while the C-terminal domain in the PmHMGR ternary complex was positioned directly over the substrate- and cofactor-binding sites in a “closed” conformation (Figure 1),

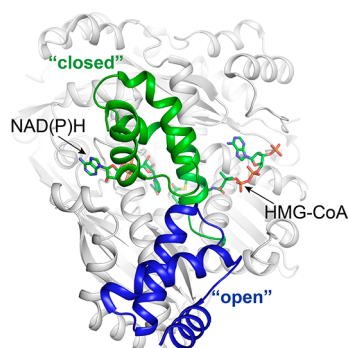


**Figure 1.** Structures of “open” and “closed” class II HMGR. Aligned crystal structures of apo-SpHMGR (PDB entry 3QAU) and the substrate- and cofactor-bound PmHMGR ternary complex (PDB entry 1QAX), representing “open” (blue) and “closed” (green) conformations of the C-terminal domain (rmsd for C<sub>α</sub> atoms of 0.80). Structures were aligned with their C-terminal domains excluded. The cofactor and substrate are labeled and shown as sticks, with C colored green, N colored blue, O colored red, P colored orange, and S colored yellow.

where the C-terminal domain contributes a catalytically essential histidine, as indicated by mutagenic and structural studies.<sup>18,20,21</sup> By alternating between “open” and “closed” conformations, the C-terminal domain might be capable of acting as a “flap” to cover the active site when the substrate and/or cofactor is bound.<sup>18</sup> However, when, how, and what triggers this C-terminal domain movement during the reaction are unknown.

To gain mechanistic insight into HMGR catalysis and to shed light on how substrate binding and cofactor binding influence the enzyme’s structure during the reaction, we first determined the cofactor preferences of SpHMGR and found that although the enzyme can use both NADH and NADPH to reduce HMG-CoA, it has a strong kinetic preference for NADPH. We also determined two crystal structures of SpHMGR, one bound with substrate HMG-CoA and one

bound with its preferred cofactor NADPH, which represents the first structure of an NADPH-bound class II HMGR. These crystal structures not only provide new structural insight into HMGR cofactor binding and specificity but also reveal new C-terminal domain conformations, allowing us to illuminate the structural movements that enable HMGR reactivity.

## ■ MATERIALS AND METHODS

**Cloning, Expression, and Purification.** A codon-optimized, linear *mvaA* gene that encodes SpHMGR (Integrated DNA Technologies) was cloned into a modified pET28b plasmid termed pSKB3, which encodes an N-terminal, TEV protease-cleavable hexahistidine tag and a kanamycin resistance cassette, using NdeI and BamHI restriction enzymes. The plasmid was transformed into *Escherichia coli* DH10B cells, and its gene sequence was confirmed (Quintara Biosciences) before its transformation into BL21(DE3) cells for protein expression.

Cells were grown in lysogeny broth supplemented with kanamycin at 37 °C until OD<sub>600</sub> reached ~0.6. Protein expression was induced with 0.5 mM isopropyl β-D-1-thiogalactopyranoside (IPTG) and proceeded for 18 h at 16 °C. Cells were harvested by centrifugation at 5000g for 10 min, flash-frozen in liquid nitrogen, and stored at –80 °C. Cells were resuspended in lysis buffer [50 mM Tris (pH 7.7), 200 mM NaCl, 10% glycerol, and 10 mM imidazole] with 0.5 unit/μL benzonase (Millipore) and 0.5 mM phenylmethanesulfonyl fluoride (PMSF) and lysed by sonication on ice at 40% amplitude for 9 min with 3 s bursts and 5 s rests. The lysate was clarified by centrifugation at maximum speed (~37000g) for 30 min at 4 °C, and the supernatant was applied to a Ni-NTA column equilibrated with lysis buffer. SpHMGR was eluted from the column in fractions using lysis buffer with 300 mM imidazole and assessed for purity by SDS–PAGE. Fractions containing the highest purity were pooled; hexahistidine-tagged TEV protease was added to cleave the hexahistidine tag from SpHMGR, and the sample was dialyzed overnight at 4 °C against 50 mM Tris (pH 7.7), 200 mM NaCl, 10% glycerol, and 0.5 mM EDTA. The sample was run over a second Ni-NTA column using lysis buffer to purify cleaved SpHMGR. The protein was further purified by gel filtration on a HiLoad 16/600 Superdex 200 prep grade column (GE Healthcare Life Sciences) equilibrated with 50 mM Tris (pH 7.7), 200 mM NaCl, and 10% glycerol using an Akta Pure chromatography system (GE Healthcare Life Sciences). Purified SpHMGR was concentrated to 15 mg/mL, flash-frozen dropwise in liquid nitrogen, and stored at –80 °C.

**Kinetic Characterization.** The cofactor specificity was assessed kinetically using a NanoDrop 2000c spectrophotometer (ThermoFisher). Each 100 μL reaction mixture at 37 °C contained 50 mM Tris (pH 7.4), 50 mM NaCl, 300 μM HMG-CoA, and 25–500 μM NAD(P)H. Reactions were initiated by the addition of 20 nM SpHMGR for NADPH reactions or 100 nM SpHMGR for NADH reactions. Enzyme-catalyzed oxidation of NAD(P)H was monitored via a decrease in absorbance at 340 nm, using an extinction coefficient of 6200 M<sup>–1</sup> cm<sup>–1</sup>. The Michaelis–Menten constant, K<sub>m</sub>, and the maximum velocity, V<sub>max</sub>, for the production of mevalonate were determined using nonlinear regression by fitting the reaction velocities to the Michaelis–Menten equation in GraphPad Prism 6.0. The values for k<sub>cat</sub> were obtained by dividing V<sub>max</sub> by the molar enzyme concentration. Values are

given as the means  $\pm$  the standard error of the mean (SEM) from triplicate experiments.

**Crystallization.** Crystallization conditions for HMG-CoA-bound SpHMGR were identified by sparse-matrix screening by sitting-drop vapor diffusion using a Crystal Gryphon (Art Robbins Instruments) with 10 mg/mL SpHMGR and 1 mM HMG-CoA. Crystals were observed under condition 17 of Crystal Screen 1 (Hampton Research), which contains 100 mM Tris (pH 8.5), 200 mM lithium sulfate, and 30% polyethylene glycol (PEG) 4000. Crystallization conditions were optimized by hanging-drop vapor diffusion with varying lithium sulfate and PEG 4000 concentrations, and small crystals grew overnight. Crystals were washed in mother liquor, crushed via vortexing, and used as seeds for microseeding. Seeded drops contained 1.0  $\mu$ L of 10 mg/mL SpHMGR with 1 mM HMG-CoA, 0.8  $\mu$ L of crystallization solution, and 0.2  $\mu$ L of the seed stock. Large crystals grew in 100 mM Tris (pH 8.5), 100–250 mM lithium sulfate, and 15–25% PEG 4000. The crystals were cryoprotected using the crystallization solution supplemented with 20% glycerol and 1 mM HMG-CoA before being flash-cooled in liquid nitrogen.

NADPH-bound SpHMGR crystals grew under the same crystallization condition that was used for the HMG-CoA-bound SpHMGR crystals. However, a new crystal form that took several weeks to grow appeared to use the HMG-CoA-bound SpHMGR microcrystals as nucleation sites for crystal growth. These rod-shaped crystals were optimized using the seeding protocol described above and co-crystallized with 2.5 mM NADPH. Large crystals grew in 100 mM Tris (pH 8.5), 100–250 mM lithium sulfate, and 30–40% PEG 4000. The crystals were cryoprotected using the crystallization solution supplemented with 20% glycerol and 5 mM NADPH before being flash-cooled in liquid nitrogen.

**X-ray Data Collection, Structure Determination, and Refinement.** X-ray diffraction data were collected at Advanced Photon Source (APS) beamline 24-ID-E. The data were indexed, merged, and scaled using iMOSFLM<sup>22</sup> in space group  $P1$  with four molecules in the asymmetric unit for the NADPH-bound structure and space group  $P2_1$  with two molecules in the asymmetric unit for the HMG-CoA-bound structure. Structures were determined by molecular replacement using Phaser<sup>23</sup> in the PHENIX suite,<sup>24</sup> where the apo-SpHMGR structure (PDB entry 3QAE) with unresolved C-terminal domains was used as the search model. Electron density maps indicated that the C-terminal domains were located in novel locations for both structures. Therefore, they were built manually in Coot<sup>25</sup> with iterations of reciprocal space refinement using phenix.refine.<sup>26</sup> After the structures were determined, we noticed that our protein contained a V355E mutational artifact. As this site is quite distant from the cofactor- and substrate-binding sites ( $>20$  Å) as well as the C-terminal domains ( $>35$  Å), we believe that this is unlikely to have a significant impact on the main findings of this paper.

## RESULTS

**Kinetic Characterization of SpHMGR.** Previous studies of SpHMGR focused on enzyme inhibition and characterized the activity using NADPH but did not examine cofactor specificity.<sup>16</sup> To determine the cofactor preference of SpHMGR, we measured steady-state kinetics with varying concentrations of either NADH or NADPH (Table 1). With respect to NADPH, SpHMGR has a  $K_m$  of  $28.9 \pm 5.1$   $\mu$ M and a  $k_{cat}$  of  $6.85 \pm 0.3$   $s^{-1}$ . With NADH, the enzyme has a  $K_m$  of

**Table 1. SpHMGR Cofactor Preferences**

	NADPH	NADH
$K_m$ ( $\mu$ M)	$28.9 \pm 5.1$	$153 \pm 59.3$
$k_{cat}$ ( $s^{-1}$ )	$6.85 \pm 0.3$	$0.131 \pm 0.02$
$k_{cat}/K_m$ ( $M^{-1} s^{-1}$ )	$2.4 \times 10^5$	$8.6 \times 10^2$

$153 \pm 59.3$   $\mu$ M and a  $k_{cat}$  of  $0.131 \pm 0.02$   $s^{-1}$ . The resulting catalytic efficiencies ( $k_{cat}/K_m$ ) are  $2.4 \times 10^5$   $M^{-1} s^{-1}$  for NADPH and  $8.6 \times 10^2$   $M^{-1} s^{-1}$  for NADH. These data show that although SpHMGR can use either cofactor for HMG-CoA reduction, NADPH is the preferred cofactor by approximately 280-fold in terms of  $k_{cat}/K_m$ , with both a lower  $K_m$  and a higher  $k_{cat}$  for NADPH compared with those of NADH.

**Overall Structures.** SpHMGR bound to its preferred cofactor NADPH crystallized in the  $P1$  space group with four molecules in the asymmetric unit, arranged as two homodimers (chains A and B and chains C and D). The overall structure is nearly identical to the prior apo-SpHMGR structures (PDB entries 3QAE and 3QAU), except for the C-terminal domains, detailed below, with root-mean-square deviations for  $C_\alpha$  atoms (rmsd's) of 0.23–0.25. Clear electron density was observed for all four monomers of the asymmetric unit, except the C-terminal domains (residues 375–424) of chains A and C were disordered. Electron density in these regions was weak and discontinuous, and thus, we did not model the C-terminal domains for chains A and C. Therefore, in the final model, chains A and C contain residues 3–372 of 424 while chains B and D contain residues 11–424 and 3–424, respectively. In addition, positive difference maps showed density in the cofactor-binding sites of both chains A and C, representing NADPH binding. For chain A, clear electron density for NADPH was observed, including for the key 2'-phosphate group, though it may be noted that the 2'-phosphate density is partially discontinuous with the rest of the NADPH molecule (Figure 2A), suggesting a small degree of disorder. For chain C, however, electron density for NADPH was significantly

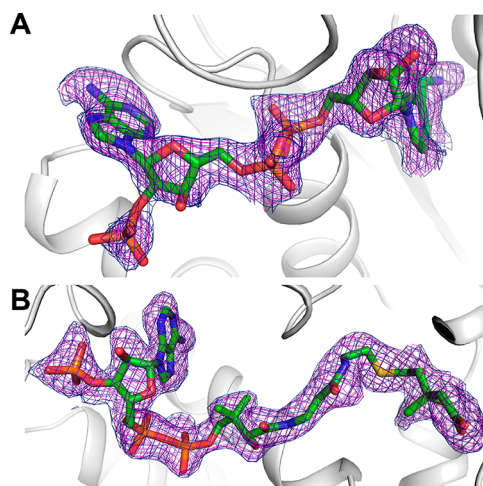


**Figure 2.** NADPH- and HMG-CoA-binding sites of SpHMGR, with  $mF_o - DF_c$  omit density for (A) NADPH and (B) HMG-CoA bound to SpHMGR (PDB entries SWPJ and 5WPK, respectively). The protein is shown as a gray cartoon; NADPH and HMG-CoA are shown as sticks, with C colored green, N colored blue, O colored red, P colored orange, and S colored yellow. The  $mF_o - DF_c$  polder omit map is contoured at  $3.0\sigma$  (pink mesh) and  $2.5\sigma$  (blue mesh), as calculated in Phenix.<sup>24,33</sup>

weaker and included significant negative  $F_O - F_C$  difference density around the nicotinamide and adenosine rings. A trial refinement at 70% occupancy for NADPH mostly satisfied the difference maps (Figure S1), but because the  $2F_O - F_C$  maps remained highly discontinuous, we chose to leave NADPH in chain C out of the final model.

SpHMGR bound to HMG-CoA crystallized in the  $P2_1$  space group with two molecules in the asymmetric unit assembled as a homodimer (chains A and B). The C-terminal domain was resolved only in chain B; therefore, in the final model, chain A contains residues 1–379 while chain B contains residues 3–424. Electron density maps showed clear density for HMG-CoA in the substrate-binding sites of both chains (Figure 2B). Complete X-ray diffraction and refinement statistics are listed in Table 2.

**Table 2. Data Collection and Refinement Statistics<sup>a</sup>**

	NADPH-bound SpHMGR	HMG-CoA-bound SpHMGR
PDB entry	5WPJ	5WPK
Diffraction Data		
beamline	APS, 24-ID-E	APS, 24-ID-E
wavelength (Å)	0.9792	0.9792
space group	P1	P21
unit cell dimensions		
<i>a</i> , <i>b</i> , <i>c</i> (Å)	58.0, 84.0, 94.2	57.9, 131.2, 57.9
$\alpha$ , $\beta$ , $\gamma$ (deg)	108.2, 100.6, 109.1	90.0, 102.5, 90.0
resolution range (Å)	72.72–2.00 (2.072–2.00)	19.23–2.30 (2.382–2.30)
Wilson <i>B</i> (Å <sup>2</sup> )	20.86	23.56
total no. of reflections	201205 (20446)	129322 (12606)
no. of unique reflections	95302 (9432)	36792 (3643)
multiplicity	2.1 (2.2)	3.5 (3.5)
completeness (%)	93.23 (92.35)	98.17 (97.98)
mean <i>I</i> / $\sigma$ ( <i>I</i> )	5.02 (1.88)	6.48 (1.84)
<i>R</i> <sub>merge</sub>	0.1159 (0.4474)	0.1514 (0.5832)
<i>R</i> <sub>meas</sub>	0.1556 (0.6014)	0.1788 (0.6913)
<i>CC</i> <sub>1/2</sub>	0.984 (0.436)	0.987 (0.676)
<i>CC</i> <sup>*</sup>	0.996 (0.779)	0.997 (0.898)
Refinement		
<i>R</i> <sub>work</sub>	0.1635 (0.2813)	0.1771 (0.2452)
<i>R</i> <sub>free</sub>	0.2236 (0.3245)	0.2333 (0.3234)
no. of protein/ligand atoms	13644	6617
rmsd for bonds (Å)	0.008	0.003
rmsd for angles (deg)	1.243	0.627
average <i>B</i> factor (Å <sup>2</sup> )	24.0	29.0
Ramachandran analysis (%)		
favored	97.72	96.87
allowed	1.90	3.13
outliers	0.38	0
MolProbity Clashscore	9.33	6.19

<sup>a</sup>Statistics for the highest-resolution shell are shown in parentheses.

In the obligate HMGR homodimer, the larger N-terminal domain, which includes the active site, forms a majority of the dimer interface. Interestingly, the interface contains an interlocking motif where residues 1–69 cross and intertwine with each other through loops formed by residues 38–58, forming an interlocked  $\beta$ -sheet that contains several conserved residues and has been observed in prior structures of HMGR

(Figure S2A,B).<sup>27,28</sup> This region is also involved in substrate binding, as in our HMG-CoA-bound SpHMGR structure Glu50 and Asn51 from the interlocking loop of one monomer interact with the adenine ring of HMG-CoA bound by the adjacent monomer (Figure S2C).

**Substrate- and Cofactor-Binding Sites.** The HMG-CoA substrate and the NAD(P)H cofactor are both long molecules that bind HMGR with their reactive groups pointing toward each other in the buried active site core at the homodimeric interface and with the rest of the molecules extending out from the active site in different directions, together resembling a “V” shape. Correspondingly, in our structure of HMG-CoA-bound SpHMGR (Figure 3A), the substrate binds with its reactive

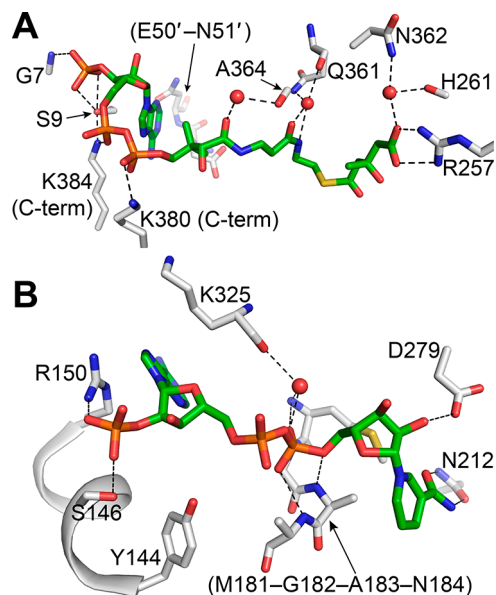


**Figure 3.** Interactions between SpHMGR and its substrate and cofactor. (A) HMG-CoA- and (B) NADPH-binding sites of SpHMGR. Protein amino acids (C colored gray) and all bound ligands (C colored green) are shown as sticks, with N colored blue, O colored red, P colored orange, and S colored yellow, and water is shown as spheres. Dashed lines represent hydrogen bonds.

HMG moiety in the active site, with Arg257 forming a salt bridge with the carboxylate of the HMG moiety, which also interacts via a water molecule with the backbone carbonyl of His261 and the side chain of Asn362. The pantothenate group of HMG-CoA then extends out toward the surface of the protein, interacting via water molecules with Gln361 and Ala364. HMG-CoA reaches the protein surface at its diphosphate group, which interacts with Lys380 and Lys384, both from the C-terminal domain. Finally, the adenosine group of HMG-CoA lies on the surface of the protein, with its adenine ring interacting with the interlocked Glu50 and Asn51 of the opposite monomer, as mentioned above. In addition, the 3'-phosphate of the adenosine ribose forms hydrogen bonds with the backbone NH group of Gly7 as well as the side chain and backbone NH group of Ser9. Interestingly, Ser9 also forms a hydrogen bond with the same Lys384 of the C-terminal domain that interacts with the substrate diphosphate, as described. Though distant in primary sequence, this Ser9–Lys384 interaction thus “bridges” the 3'-phosphate and the diphosphate groups of HMG-CoA. In addition, there are several hydrophobic interactions between the pantothenate

and  $\beta$ -mercaptoethylamine moieties of HMG-CoA and the enzyme, including its C-terminal domain.

In our NADPH-bound SpHMGR structure (Figure 3B), only one NADPH molecule is included in the final model. Although the active site lies at the dimer interface, the cofactor interacts almost exclusively with the opposite monomer as HMG-CoA. As with the substrate, the cofactor binds with its reactive group buried in the active site. Here, the amide group of the nicotinamide ring hydrogen bonds with Asn212, while the 2'-OH group of the nicotinamide's ribose hydrogen bonds with Asp279. From here, the cofactor, like the substrate, extends out toward the protein surface and reaches the solvent at its diphosphate moiety, which interacts directly or through bridging water molecules with the backbone NH groups of Met181, Gly182, Ala183, and Asn184. Together, these four residues form the N-terminal cap of a helix and its preceding loop. The NADPH adenosine group is solvent-exposed, with the adenine ring sandwiched between stacking Lys325 and Arg150 side chains. Intriguingly, Arg150 also forms a salt bridge with the critical 2'-phosphate of NADPH, which also interacts with Ser146 (Figure 3B).

**C-Terminal Domain.** In our NADPH-bound SpHMGR structure, the resolved C-terminal domains of chains B and D are both positioned in "open" conformations, in that they are flipped away from the active site, leaving the substrate- and cofactor-binding sites exposed. However, the C-terminal domains in this structure adopt "open" conformations slightly different from each other (Figure 4A, light and dark orange). Moreover, neither conformation aligns with the previously observed "open" C-terminal domain of the apo-SpHMGR structure (PDB entry 3QAU) (Figure 4A, blue). These

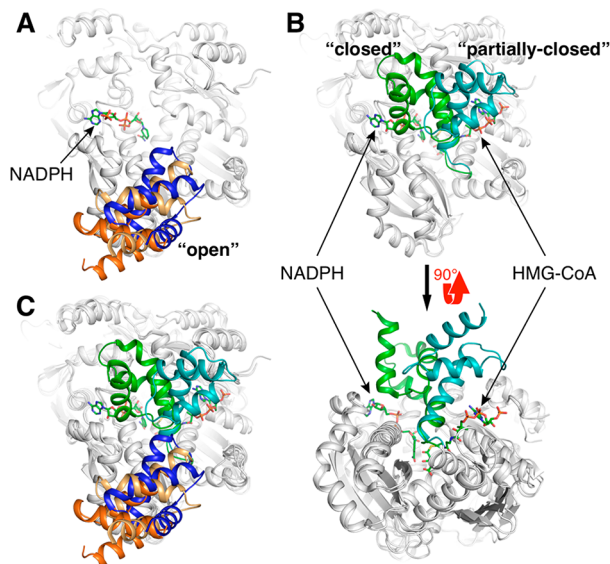


**Figure 4.** Conformational movements of the C-terminal domain. (A) Alignment of apo-SpHMGR (PDB entry 3QAU) with chain B and chain D of the NADPH-bound SpHMGR structure, with C-terminal domains colored blue, light orange, and dark orange (rmsd's of 0.23 and 0.25). (B) Alignment of HMG-CoA-bound SpHMGR, with the C-terminal domain colored teal, with the HMG-CoA- and NAD<sup>+</sup>-bound PmHMGR ternary complex (PDB entry 1QAX), with the C-terminal domain colored green (rmsd of 0.89). (C) Overlay of panels A and B. Proteins are shown as gray cartoons, except for C-terminal domains. All ligands are shown as sticks, with C colored green, N colored blue, O colored red, P colored orange, and S colored yellow.

variations in "open" C-terminal domain conformations appear to be caused by interactions with adjacent molecules in the crystal.

On the other hand, the C-terminal domain in our HMG-CoA-bound SpHMGR structure is observed in an entirely new position (Figure 4B). Although flipped more toward the active site relative to the "open" conformations, the C-terminal domain is not positioned over the cofactor-binding site, as was previously observed in the "closed" structures of the PmHMGR ternary complex (Figure 4B). In the "closed" conformation, the C-terminal domain covers both the substrate and the cofactor (Figure 4B, bottom panel), while also contacting the N-terminal domain of the adjacent monomer. Instead, the C-terminal domain in our substrate-bound SpHMGR structure is rotated by approximately 90° from the N-terminal domain of the adjacent monomer and from the cofactor-binding site, as well. In this new position, the C-terminal domain still covers the substrate-binding site; indeed, C-terminal domain residues Lys380 and Lys384 both directly interact with the CoA portion of the substrate (Figures 3A and 5), as described above. Therefore, we term this novel

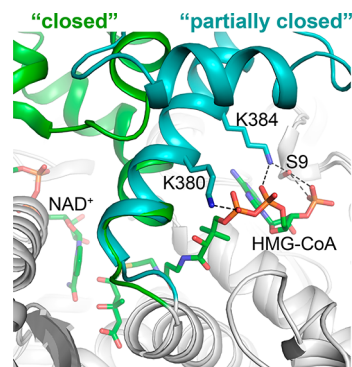


**Figure 5.** Close-up view of the class II HMGR C-terminal domain in the "closed" conformation colored green (from the PmHMGR ternary complex, PDB entry 1QAX) and the "partially closed" conformation colored teal (from the HMG-CoA-bound SpHMGR presented here, PDB entry 5WPK) from Figure 4B (bottom panel). Salt bridge and hydrogen bonding interactions between the "partially closed" C-terminal domain and the HMG-CoA substrate are shown as dashed lines.

position the "partially closed" conformation of the C-terminal domain, which covers the substrate-binding site while leaving the cofactor-binding site open (Figures 4B and 5). Despite the C-terminal domain maintaining direct contact with the CoA moiety in this "partially closed" conformation, the catalytic histidine (His378 in SpHMGR) is lifted slightly and tilted away from CoA compared with that in the "closed" PmHMGR ternary structure (Figure S3).

## DISCUSSION

HMGR is a key enzyme in the mevalonate pathway, which is responsible for the biosynthesis of a wide range of molecules, from cholesterol and other steroids to isoprenoid natural products, many of which have medicinal or other uses as commodity chemicals. In particular, microbial class II HMGRs display a wide range of NAD(P)H cofactor specificities, where some enzymes use either NADH or NADPH exclusively, while others can employ both cofactors to reduce HMG-CoA to mevalonate and CoA. Cofactor usage is a great concern in

metabolic engineering for the production of commodity chemicals, including isoprenoid-derived drugs and biofuels,<sup>29,30</sup> to ensure and maintain redox balance and the availability of the correct reductant, either NADH or NADPH. Therefore, a better understanding of the HMGR reaction mechanism and cofactor specificity may lead to the development of HMGR variants whose cofactor preferences are optimized to address issues of redox balance in microorganisms engineered for isoprenoid production via the mevalonate pathway.<sup>31</sup> In addition, greater insight into the reaction mechanism and cofactor preferences of class II HMGR could lead to the development of novel antibiotics, as class II HMGRs are present only in bacteria and archaea. Indeed, the mevalonate pathway has been shown to be essential for growth in many pathogenic microorganisms, including *S. pneumoniae*, a major cause of pneumonia.<sup>32</sup>

We demonstrate here that class II HMGR from *S. pneumoniae* can utilize both NADPH and NADH, but with a strong preference for NADPH ( $k_{\text{cat}}/K_m$  of  $2.4 \times 10^5 \text{ M}^{-1} \text{ s}^{-1}$  for NADPH vs  $8.6 \times 10^2 \text{ M}^{-1} \text{ s}^{-1}$  for NADH). Therefore, we determined the crystal structure of SpHMGR in the presence of NADPH to better understand the structural basis of cofactor specificity, representing the first structure of a class II HMGR bound to NADPH.

In a prior structure of NADH-bound PmHMGR,<sup>18</sup> Asp146 hydrogen bonds with the NADH adenosine 2'-OH group, presumably preventing the larger and negatively charged 2'-phosphate of NADPH from binding to the enzyme. This observation led to the possibility that Asp146 confers cofactor specificity in PmHMGR; however, its mutation to alanine, glycine, asparagine, or serine did not switch the cofactor preference,<sup>4</sup> as the catalytic efficiency,  $k_{\text{cat}}/K_M$ , for NADH was still 10–1000-fold greater than for NADPH, indicating that Asp146 in PmHMGR is not solely responsible for cofactor specificity.

Surprisingly, in structures of NADPH-preferring SpHMGR, Asp146 of PmHMGR is not replaced by a smaller or positively charged residue to accommodate the 2'-phosphate of NADPH, but with a bulky and neutral residue (Tyr144). In fact, we observe that Asp146 of PmHMGR and Tyr144 of SpHMGR are both the first amino acids of a short, seven-residue conserved helix that binds the NAD(P)H cofactor at its adenosine moiety (Figure 6). This helix, which we term the “cofactor helix”, has a completely different sequence in PmHMGR (residues 146–152) and SpHMGR (residues 144–150) (DQLLNSL and YPSIVKR, respectively).

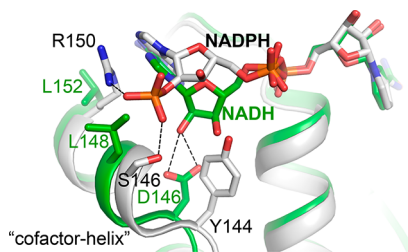


**Figure 6.** Comparison of NADH and NADPH cofactor-binding sites of class II HMGR. Alignment of the HMG-CoA- and NAD<sup>+</sup>-bound PmHMGR ternary complex (green, with residue labels in green) with the NADPH-bound SpHMGR structure (gray, with residue labels in black). The “cofactor helix” is labeled, and dashed lines represent hydrogen bonds.

Because of its preference for NADPH over NADH, replacing Asp146 of PmHMGR with the bulkier and uncharged Tyr144 of SpHMGR may at first seem counterintuitive. However, in our cofactor-bound SpHGMR structure, Tyr144 prevents the NADPH adenosine ribose from occupying the same space as observed with NADH in PmHMGR (Figure 6). Instead, because of the large size of tyrosine, the NADPH adenosine is shifted in the cofactor-binding site compared to NADH in PmHMGR. Though the nicotinamide rings and the diphosphates of NADH and NADPH align well between the PmHMGR and SpHMGR structures, the phosphoribose in SpHMGR is shifted by  $\sim 3.0 \text{ \AA}$ , causing the adenine ring also to be displaced by  $\sim 2.0 \text{ \AA}$ . Therefore, it appears unlikely that NADPH of SpHMGR could occupy the same space as NADH in PmHMGR, because of the steric hindrance of Tyr144. As a result, Tyr144 blocks phosphoribose from getting close to the start of the cofactor helix, thus providing space for the 2'-phosphate to interact with Ser146 instead, which is located toward the center of the cofactor helix. In fact, this serine residue appears to be highly conserved among HMGRs that prefer NADPH, while HMGRs that prefer NADH have a hydrophobic residue at this position (Figure 7), such as Leu148 in PmHMGR. Furthermore, the adenosine ribose of NADPH has shifted enough to allow Arg150 at the end of the SpHMGR cofactor helix to play a dual role by interacting with both the 2'-phosphate and the adenine ring, as described above. However, in NADH-preferring HMGRs, a hydrophobic residue is often found in this position instead of arginine (Figure 7), such as Leu152 in PmHMGR.

Taken together, these structural observations suggest that several residues of the cofactor helix contribute to NADPH binding and recognition in class II HMGRs. In SpHMGR, the bulky Tyr144 causes a shift in the location of the adenosine moiety of NADPH as compared to that of NADH in PmHMGR (Figure 6). This shift allows the 2'-phosphate of NADPH to interact with both conserved Ser146 in the center of the cofactor helix and conserved Arg150 at the end of the helix, which also stacks with the NADPH adenine ring. With these NADPH-binding features now described, future studies to modify this region may offer additional insight into how cofactor specificity may be controlled or engineered.

In addition, our SpHMGR structures reveal large conformational changes upon substrate binding. The C-terminal domain is disordered and absent in most HMGR crystal structures but has been visualized in the structures of apo-SpHMGR and the ternary PmHMGR complex, bound simultaneously with both the cofactor and substrate or substrate analogue. These studies indicated that this domain may act as a flexible flap that can open and close over the active site at some point during the reaction.<sup>18</sup> In our NADPH-bound SpHMGR structure, the two resolved C-terminal domains are positioned in “open” conformations that are slightly different from each other (Figure 4A), likely because of crystal packing. This suggests that the C-terminal domain does not occupy a single, rigid “open” conformation but is flexible and can sample many possible “open” positions that are all distant from the cofactor- and substrate-binding sites. Such flexibility also explains why this domain is often unresolved in HMGR crystal structures. Importantly, these “open” conformations are observed regardless of whether the cofactor is bound, as in our NADPH-bound structure, or unbound, as in the prior apo-SpHMGR structure (PDB entry 3QAE). Indeed, the partial occupancy for NADPH observed in chain C of our NADPH-

Organism	cofactor-helix	Cofactor preference
<i>B. cenocepacia</i>	...LANSRDKVVLVGLGGGCRDI...	NADH
<i>P. mevalonii</i>	...LANRKDQLNSLGGGCRDI...	NADH
<i>D. acidovorans</i>	...RANSRDKVLIGLGGGCKDI...	NADH
<i>B. petrii</i>	...LCDDCDPLLVKLGGLQDV...	NADH
<i>A. fulgidus</i>	...RANECDPMLVNLGGGCKDI...	NADH>NADPH
<i>S. aureus</i>	...IADEAYPSIKARGGGYQRI...	NADPH>NADH
<i>L. monocytogenes</i>	...IANQAHPSLQKRGGGAVKI...	NADPH>NADH
<i>S. pneumoniae</i>	...LANQAYPSIVKRGGGARDL...	NADPH>NADH
<i>E. faecalis</i>	...QAELSYPSIVKRGGLRDL...	NADPH
<i>B. burgdorferi</i>	...WIEPLLINMNRGGGFRL...	NADPH

**Figure 7.** Sequence alignment of class II HMGRs. An alignment of cofactor helix sequences (boxed) for class II HMGRs from different organisms is shown alongside known cofactor preferences. NADH-preferring enzymes contain aspartate, a hydrophobic residue, and leucine in the first, third, and final positions of the cofactor helix, respectively. Meanwhile, in NADPH-preferring enzymes, these three positions are occupied by an aromatic or large hydrophobic residue, a small polar residue (often serine), and arginine, respectively. Class II HMGR sequences and preferences are listed as follows: *B. cenocepacia*,<sup>5</sup> *P. mevalonii*,<sup>4</sup> *Delftia acidovorans*,<sup>31</sup> *Bordetella petrii*,<sup>31</sup> *A. fulgidus*,<sup>9</sup> *St. aureus*,<sup>7</sup> *L. monocytogenes*,<sup>8</sup> *S. pneumoniae* (this work), *E. faecalis*,<sup>6</sup> and *Borrelia burgdorferi*.<sup>34</sup>

bound structure and the slightly weaker density for NADPH in chain A are consistent with the notion that these “open” conformations allow for cofactor entry and exit.

Although NADPH binding alone does not appear to trigger movement of the C-terminal domain to the “closed” conformation, in our substrate-bound SpHMGR structure the C-terminal domain adopts a new, “partially closed” conformation (Figure 4B). This structure represents the first visualization the HMGR C-terminal domain in which the substrate is bound in the absence of the cofactor. Compared to the fully “closed” conformation depicted in the structures of the PmHMGR ternary complex,<sup>19</sup> the C-terminal domain is rotated ~90° away from the cofactor-binding site and toward the HMG-CoA-binding site (Figure 4B), with multiple interactions observed between the “partially closed” C-terminal domain and the CoA moiety. Therefore, in this position, the cofactor-binding site is left open and accessible while the substrate-binding site remains closed off by the C-terminal domain (Figures 4B and 5).

The discovery of this “partially closed” conformation might also help to explain how class II HMGRs can undergo cofactor exchange during the reaction cycle without releasing the reaction intermediates mevaldyl-CoA or mevaldehyde, by using a mobile C-terminal domain that adopts multiple conformations (Figure 4C). In this proposed model, before substrate binding, the C-terminal domain is “open” and flexible, regardless of whether the cofactor is bound, as described above and observed in the prior apo-SpHMGR structure and the NADPH-bound SpHMGR structure presented here. When both the substrate and the cofactor are bound, the C-terminal domain closes over both sites and contributes a catalytically essential histidine residue, as seen in structures of the “closed” PmHMGR ternary complex.<sup>18,19</sup> After the first reduction step that forms NAD(P)<sup>+</sup> and the mevaldyl-CoA intermediate, the C-terminal domain rotates away from the cofactor-binding site to the new “partially closed” conformation, which allows for cofactor exchange while keeping the intermediate bound to the enzyme through a number of interactions between the C-terminal domain and the CoA group, as depicted in our HMG-CoA-bound SpHMGR structure. After cofactor exchange is complete and the second NAD(P)H molecule binds, the C-terminal domain can fully close over both cofactor- and substrate-binding sites again, and the second reduction step can proceed. When the

reaction is complete, the C-terminal domain can swing open once again to allow for product and cofactor release.

In conclusion, the two crystal structures of SpHMGR described here provide new insight into both the reaction mechanism and the structural basis of cofactor preference in class II HMGR. The crystal structure of NADPH-bound SpHMGR is the first structure of a class II HMGR bound to NADPH, enabling identification and examination of how residues in the “cofactor helix”, present only in microbial class II enzymes, contribute to NAD(P)H cofactor binding and recognition. This structure also demonstrates the inherent flexibility of the C-terminal domain in the “open” conformation, which is observed regardless of whether the cofactor is bound. Meanwhile, the crystal structure of HMG-CoA bound to SpHMGR reveals a new “partially closed” conformation for the C-terminal domain, which suggests how substrate binding may trigger movement of the C-terminal domain from the “open” conformation toward the active site. By covering the substrate-binding site while leaving the cofactor-binding site open, this “partially closed” conformation also illuminates the structural basis for how class II HMGRs can accomplish cofactor exchange during the reaction without the premature and wasteful release of intermediates. With these newly identified conformations of the enzyme, additional studies, including those that investigate intermediate binding in HMGR, may be performed to further probe the conformational landscape of this important enzyme.

## ■ ASSOCIATED CONTENT

### 📄 Supporting Information

The Supporting Information is available free of charge on the ACS Publications website at DOI: 10.1021/acs.biochem.7b00999.

Supporting figures that depict electron density following a trial refinement of NADPH in chain C, the interlocking region of the SpHMGR homodimer, and a close-up comparison of the catalytic histidine position in “closed” and “partially closed” conformations of the C-terminal domain (PDF)

## ■ AUTHOR INFORMATION

### Corresponding Author

\*E-mail: ykung@brynawr.edu.

ORCID 

Yan Kung: 0000-0002-6132-7969

## Author Contributions

Y.K. conceived of the project and designed the experiments with B.R.M., who carried out the kinetic and crystallographic work and determined and refined the X-ray structures. Y.K. and B.R.M. analyzed the data and wrote the paper.

## Funding

This work was supported by the National Institutes of Health (GM116029), Bryn Mawr College, the K/G Fund for Faculty Research, and the Howard Hughes Medical Institute.

## Notes

The authors declare no competing financial interest.

## ACKNOWLEDGMENTS

This work is based upon research conducted at the Northeastern Collaborative Access Team beamlines, which are funded by the National Institute of General Medical Sciences of the National Institutes of Health (P41 GM103403). The Eiger 16M detector on beamline 24-ID-E is funded by a NIH-ORIP HEI grant (S10OD021527). This research used resources of the Advanced Photon Source, a U.S. Department of Energy (DOE) Office of Science User Facility operated for the DOE Office of Science by Argonne National Laboratory under Contract DE-AC02-06CH11357.

## ABBREVIATIONS

HMG-CoA, 3-hydroxy-3-methylglutaryl coenzyme A; HMGR, HMG-CoA reductase; PDB, Protein Data Bank; APS, Advanced Photon Source; IPTG, isopropyl  $\beta$ -D-1-thiogalactopyranoside; PMSF, phenylmethanesulfonyl fluoride; NTA, nitrilotriacetic acid; SDS-PAGE, sodium dodecyl sulfate-polyacrylamide gel electrophoresis; PEG, polyethylene glycol; rmsd, root-mean-square deviation.

## REFERENCES

- (1) Bochar, D. A., Stauffacher, C. V., and Rodwell, V. W. (1999) Sequence comparisons reveal two classes of 3-hydroxy-3-methylglutaryl coenzyme A reductase. *Mol. Genet. Metab.* 66, 122–127.
- (2) Friesen, J. A., and Rodwell, V. W. (2004) The 3-hydroxy-3-methylglutaryl coenzyme-A (HMG-CoA) reductases. *Genome Biol.* 5, 248.
- (3) Hedl, M., Taberero, L., Stauffacher, C. V., and Rodwell, V. W. (2004) Class II 3-hydroxy-3-methylglutaryl coenzyme A reductases. *J. Bacteriol.* 186, 1927–1932.
- (4) Friesen, J. A., Lawrence, C. M., Stauffacher, C. V., and Rodwell, V. W. (1996) Structural determinants of nucleotide coenzyme specificity in the distinctive dinucleotide binding fold of HMG-CoA reductase from *Pseudomonas mevalonii*. *Biochemistry* 35, 11945–11950.
- (5) Schwarz, B. H., Driver, J., Peacock, R. B., Dembinski, H. E., Corson, M. H., Gordon, S. S., and Watson, J. M. (2014) Kinetic characterization of an oxidative, cooperative HMG-CoA reductase from *Burkholderia cenocepacia*. *Biochim. Biochim. Biophys. Acta, Proteins Proteomics* 1844, 457–464.
- (6) Hedl, M., Sutherlin, A., Wilding, E. I., Mazzulla, M., McDevitt, D., Lane, P., Burgner, J. W., II, Lehnbeuter, K. R., Stauffacher, C. V., Gwynn, M. N., and Rodwell, V. W. (2002) *Enterococcus faecalis* acetoacetyl-coenzyme A thiolase/3-hydroxy-3-methylglutaryl-coenzyme A reductase, a dual-function protein of isopentenyl diphosphate biosynthesis. *J. Bacteriol.* 184, 2116–2122.
- (7) Wilding, E. I., Kim, D. Y., Bryant, M. N., Gwynn, R. D., Lunsford, D., McDevitt, J. E., Myers, J. E., Jr., Rosenberg, M., Sylvester, D., Stauffacher, C. V., and Rodwell, V. W. (2000)

Essentiality, expression, and characterization of the class II 3-hydroxy-3-methylglutaryl coenzyme A reductase of *Staphylococcus aureus*. *J. Bacteriol.* 182, 5147–5152.

- (8) Theivagt, A. E., Amanti, E. N., Beresford, J. N., Taberero, L., and Friesen, J. A. (2006) Characterization of an HMG-CoA reductase from *Listeria monocytogenes* that exhibits dual coenzyme specificity. *Biochemistry* 45, 14397–14406.

- (9) Kim, D.-Y., Stauffacher, C. V., and Rodwell, V. W. (2000) Dual coenzyme specificity of *Archaeoglobus fulgidus* HMG-CoA reductase. *Protein Sci.* 9, 1226–1234.

- (10) Haines, B. E., Wiest, O., and Stauffacher, C. V. (2013) The increasingly complex mechanism of HMG-CoA reductase. *Acc. Chem. Res.* 46, 2416–2426.

- (11) Jordan-Starch, T. C., and Rodwell, V. W. (1989) *Pseudomonas mevalonii* 3-hydroxy-3-methylglutaryl-CoA reductase: Characterization and chemical modification. *J. Biol. Chem.* 264, 17913–17918.

- (12) Rétey, J., von Stetten, E., Coy, U., and Lynen, F. (1970) A probable intermediate in the enzymic reduction of 3-hydroxy-3-methylglutaryl coenzyme A. *Eur. J. Biochem.* 15, 72–76.

- (13) Bensch, W. R., and Rodwell, V. W. (1970) Purification and properties of 3-hydroxy-3-methylglutaryl coenzyme A reductase from *Pseudomonas*. *J. Biol. Chem.* 245, 3755–3762.

- (14) Durr, I. F., and Rudney, H. (1960) The reduction of  $\beta$ -hydroxy- $\beta$ -methylglutaryl coenzyme A to mevalonic acid. *J. Biol. Chem.* 235, 2572–2578.

- (15) Ferguson, J. J., Jr., Durr, I. F., and Rudney, H. (1959) The biosynthesis of mevalonic acid. *Proc. Natl. Acad. Sci. U. S. A.* 45, 499–504.

- (16) Feng, L., Zhou, L., Sun, Y., Gui, J., Wang, X., Wu, P., Wan, J., Ren, Y., Qiu, S., Wei, X., and Li, J. (2011) Specific inhibitions of annonaceous acetogenins on class II 3-hydroxy-3-methylglutaryl coenzyme A reductase from *Streptococcus pneumoniae*. *Bioorg. Med. Chem.* 19, 3512–3519.

- (17) Lawrence, C. W., Rodwell, V. W., and Stauffacher, C. V. (1995) Crystal structure of *Pseudomonas mevalonii* HMG-CoA reductase at 3.0 angstrom resolution. *Science* 268, 1758–1762.

- (18) Taberero, L., Bochar, D. A., Rodwell, V. W., and Stauffacher, C. V. (1999) Substrate-induced closure of the flap domain in the ternary complex structures provides insights into the mechanism of catalysis by 3-hydroxy-3-methylglutaryl-CoA reductase. *Proc. Natl. Acad. Sci. U. S. A.* 96, 7167–7171.

- (19) Steussy, C. N., Critchlow, C. J., Schmidt, T., Min, J.-K., Wrenford, L. V., Burgner, J. W., II, Rodwell, V. W., and Stauffacher, C. V. (2013) A novel role for coenzyme A during hydride transfer in 3-hydroxy-3-methylglutaryl-coenzyme A reductase. *Biochemistry* 52, 5195–5205.

- (20) Darnay, B. G., Wang, Y., and Rodwell, V. W. (1992) Identification of the catalytically important histidine of 3-hydroxy-3-methylglutaryl-coenzyme A reductase. *J. Biol. Chem.* 267, 15064–15070.

- (21) Darnay, B. G., and Rodwell, V. W. (1993) His865 is the catalytically important histidyl residue of Syrian hamster 3-hydroxy-3-methylglutaryl-coenzyme A reductase. *J. Biol. Chem.* 268, 8429–8435.

- (22) Batty, T. G., Kontogiannis, L., Johnson, O., Powell, H. R., and Leslie, A. G. (2011) iMOSFLM: a new graphical interface for diffraction-image processing with MOSFLM. *Acta Crystallogr., Sect. D: Biol. Crystallogr.* 67, 271–281.

- (23) McCoy, A. J., Grosse-Kunstleve, R. W., Adams, P. D., Winn, M. D., Storoni, L. C., and Read, R. J. (2007) Phaser Crystallographic Software. *J. Appl. Crystallogr.* 40, 658–674.

- (24) Adams, P. D., Afonine, P. V., Bunkóczi, G., Chen, V. B., Davis, I. W., Echols, N., Headd, J. J., Hung, L.-W., Kapral, G. J., Grosse-Kunstleve, R. W., McCoy, A. J., Moriarty, N. W., Oeffner, R., Read, R. J., Richardson, D. C., Richardson, J. S., Terwilliger, T. C., and Zwart, P. H. (2010) PHENIX: a comprehensive Python-based system for macromolecular structure solution. *Acta Crystallogr., Sect. D: Biol. Crystallogr.* 66, 213–221.

(25) Emsley, P., and Cowtan, K. (2004) Coot: model-building tools for molecular graphics. *Acta Crystallogr., Sect. D: Biol. Crystallogr.* 60, 2126–2132.

(26) Afonine, P. V., Grosse-Kunstleve, R. W., Echols, N., Headd, J. J., Moriarty, N. W., Mustyakimov, M., Terwilliger, T. C., Urzhumtsev, A., Zwart, P. H., and Adams, P. D. (2012) Towards automated crystallographic structure refinement with phenix.refine. *Acta Crystallogr., Sect. D: Biol. Crystallogr.* 68, 352–367.

(27) Istvan, E. S., Palnitkar, M., Buchanan, S. K., and Deisenhofer, J. (2000) Crystal structure of the catalytic portion of human HMG-CoA reductase: insights into regulation of activity and catalysis. *EMBO J.* 19, 819–830.

(28) Istvan, E. S. (2001) Bacterial and mammalian HMG-CoA reductase: related enzymes with distinct architectures. *Curr. Opin. Struct. Biol.* 11, 746–751.

(29) Kung, Y., Runguphan, W., and Keasling, J. D. (2012) From fields to fuels: recent advances in the microbial production of biofuels. *ACS Synth. Biol.* 1, 498–513.

(30) George, K. W., Alonso-Gutierrez, J., Keasling, J. D., and Lee, T. S. (2015) Isoprenoid drugs, biofuels, and chemicals—artemisinin, farnesene, and beyond. *Adv. Biochem. Eng./Biotechnol.* 148, 355–389.

(31) Ma, S. M., Garcia, D. E., Redding-Johanson, A. M., Friedland, G. D., Chan, R., Batth, T. S., Haliburton, J. R., Chivian, D., Keasling, J. D., Petzold, C. J., Soon Lee, T., and Chhabra, S. R. (2011) Optimization of a heterologous mevalonate pathway through the use of variant HMG-CoA reductases. *Metab. Eng.* 13, 588–597.

(32) Wilding, E. I., Brown, J. R., Bryant, A. P., Chalker, A. F., Holmes, D. J., Ingraham, K. A., Iordanescu, S., So, C. Y., Rosenberg, M., and Gwynn, M. N. (2000) Identification, evolution, and essentiality of the mevalonate pathway for isopentenyl diphosphate biosynthesis in gram-positive cocci. *J. Bacteriol.* 182, 4319–4327.

(33) Liebschner, D., Afonine, P. V., Moriarty, N. W., Poon, B. K., Sobolev, O. V., Terwilliger, T. C., and Adams, P. D. (2017) Polder maps: improving OMIT maps by excluding bulk solvent. *Acta Crystallogr., Sect. D: Biol. Crystallogr.* 73, 148–157.

(34) Van Laar, T. A., Lin, Y.-H., Miller, C. L., Karna, S. L. R., Chambers, J. P., and Seshu, J. (2012) Effect of levels of acetate on the mevalonate pathway of *Borrelia burgdorferi*. *PLoS One* 7, No. e38171.